

Persistence diagrams as morphological signatures of cells: A method to measure and compare cells within a population

Yossi Bokor Bleile^{1,2*}, Pooja Yadav³, Patrice Koehl⁴, Florian Rehfeldt³

1 Institute of Science and Technology Austria, Klosterneuburg, Austria

2 School of Mathematics and Statistics, The University of Sydney, Sydney, NSW, Australia

3 Experimental Physics I, University of Bayreuth, Bayreuth, Germany

4 Department of Computer Science, University of California, Davis, California, America

* yossi.bokorbleile@ista.ac.at (YBB)

Abstract

Quantifying cellular morphology is a common approach in life sciences to study regulatory mechanisms, cell fate, homeostasis, and pathologies. However, inherent heterogeneities within cell populations can render traditional automated microscopy image analysis methods unreliable or even impossible. This often leads to manual inspection and pseudo-quantitative evaluation of cell images, which is prone to user bias and not readily reproducible. To address these challenges, we developed a computational framework based on topological data analysis (TDA) to investigate and quantify cell morphology heterogeneity with two sample sets exemplifying common cases in cell biology: human adult mesenchymal stem cells, which are primary cells derived from a patient, and HeLa cells, an immortalised cell line. Our approach is based on the characterisation of the shape of the cell by its contour and the position of its nucleus. We build a filtering of the edges defining the contour using a radial distance function initiated from the nucleus. This filtering is then used to construct a persistence diagram that serves as a signature of the cell shape. Two cells can then be compared by computing the Wasserstein distance between their persistence diagrams. Given a cell population, we then compute a distance matrix that includes all pairwise distances between its members. We analyse this distance matrix using hierarchical clustering with different linkage schemes and define a purity score that quantifies consistency between those different schemes, which can then be used to assess homogeneity within the cell population. We illustrate and validate our approach by identifying sub-populations in human mesenchymal stem cell populations, and analysing the heterogeneity of a population of HeLa cells.

Author summary

The fundamental units of life are cells, and understanding how they grow, divide, die, and change shape is of central importance in many areas of the life sciences. In this paper, we focus on how to define and compare the shape of cells. We identify the shape of a cell with its contour (i.e. location of its membrane) supplemented with the position of its nucleus. We use topological data analysis to define a signature of that shape, generated from its persistent homology, a mathematical construction that reflects the

relative position of the nucleus with respect to segments of the contours. We compute the distance between two cells as the Wasserstein distance between their shape signatures. Using this distance, we analyse populations of cells to help identify members with unusual shapes (usually referred to as outliers) as well as sub-populations. We validate our approach to identify sub-populations within human mesenchymal stem cell populations that are known to be heterogeneous, and search for outliers in a population of HeLa cells.

1 Introduction

Cells are the basic unit of life. Understanding how they grow, divide, die, and change shape is of central importance in virtually all fields of cell biology, including immunology, cancer biology, pathology, tissue, and organ morphogenesis during development, as well as in many other areas of the life sciences. Of significance to most studies aimed at these understandings is the concept of shape. The shape of a cell is defined by the geometric constraints of the space it occupies and is determined by the external boundaries and positions of the internal components. The shape is the result of the mechanical balance of forces exerted on the cell membrane by intra-cellular components and the extra-cellular environment. It is a geometric property controlled by a variety of biochemical pathways. Cell biologists study in parallel the morphology of cells (their geometry) with the regulation mechanisms that modify this morphology. These studies benefit from recent advances in microscopy and image processing techniques. Current microscopes provide 2D images that make it possible to study cellular shapes, or more precisely 2D projections of cellular shapes. The question remains as to how to measure and compare these shapes. This paper focusses on a new technique for performing these analyses.

Our interest in 2D shape comparisons is initially motivated by a seminal paper by Engler et al. that demonstrated that the mechanical properties of the extracellular matrix dictate the differentiation of human mesenchymal stem cells (hMSCs) towards various lineages [1]. While the up- and down-regulation of genes and transcription factors towards terminal differentiation take up to several days or even weeks, experiments focused on the first 24 hours of hMSCs after seeding on a substrate showed a significant impact of matrix rigidity on the structural formation of acto-myosin stress fibres. Those studies introduced an order parameter S that could be used as an early morphological descriptor of mechano-directed stem cell differentiation [2, 3].

The analysis described above was based on the filamentous structure of the cytoskeleton and its pattern formation; instead, we focus on the global cell morphology, in particular, the outline of the cellular cortex in two dimensions. Our goal is to use this morphology to identify possible differences in a cell population. For example, hMSCs are primary cells, collected from the bone marrow of human individuals in contrast to HeLa cells, an immortalised cell line. This leads to an intrinsic diversity for the cell population that is additionally influenced by potential sub-populations of bone marrow fibroblasts (roughly 5%) [4, 5]. Our aim is to see if geometry alone allows us to identify those sub-populations within a sample of cells.

A 2D shape is defined as a domain D in \mathbb{R}^2 , delimited by its boundary, ∂D , often referred to as the contour of D . In all our applications, we will take the contour to be a piecewise smooth or polygonal Jordan curve, that is, a simple closed curve in \mathbb{R}^2 . There are multiple geometric representations of such 2D shapes, leading to different methods for their characterisations. We briefly review two such representations.

In the *digital image* representation, common to most real applications, raw data are provided in the form of 2D images (see Figure 1A). In essence, the data to be understood and compared is a collection of pixels. Traditional methods of comparing



Fig 1. (A) Fluorescence microscopy image of a human mesenchymal stem cell (hMSC), scale bar represents 100 μm . (B) Fluorescence microscopy image of the corresponding nucleus. (C) Plot of the corresponding contour of that cell with the centre of the cell shown as a red dot.

such images usually proceed in three steps. They first define a set of well-chosen landmarks or key points on the surfaces of the shapes, then assign “signatures” to these key points (coordinates in a parameterising domain), and finally determine a map maximising the correspondence of signatures (for a review, see [6]). With the increase in computing power and the large number of image data sets that are generated, these ideas are often studied in the context of deep learning, where the key points and signatures are learnt from large data sets. Deep learning has become the predominant method used in 2D image analysis (see [7] for a review of applications to medical image analysis). However, its applicability requires access to large data sets. In many cases, limited numbers of images are available, either because they are expensive to produce or because they model a rare phenomenon. This is the case for the stem cell images considered in this paper. In addition, deep learning remains something of a black-box procedure for classification. Cell biologists seek to understand the interplay between the geometry of a cell and the biochemical processes that are responsible for this geometry. They need a finer and more mechanistic understanding of the processes that drive shape, requiring mathematical approaches.

A second representation of 2D shapes, which we refer to as *shape as planar contour*, is based on the curve describing the outer boundary of the shape (see Figure 1C). This is well suited to applications focused on the geometric configuration of a shape, where factors such as the colour or grey level of the interior are either not relevant or not available. Methods for modelling the similarity between two shapes given as planar contours have been based on defining a distance between two curves in the plane. The proposed distances include the Hausdorff and Fréchet distances [8]. Other techniques are based on the Poisson equation [9], integral invariants [10], and an elastic shape distance on the energy required to elastically deform one boundary contour to the other [11, 12].

Paraphrasing a recent review paper by D. Chitwood and colleagues, “Shape is data and data is shape” [13]. As described above, shape is a signature of biological objects such as cells discussed above, that are significant for their biological functions. As such, shape characteristics are integral parts of the data that represent these biological objects. In contrast, there is a geometric structure within the data that is referred to as the shape of the data. Analysing the shape of data has become an essential section of data science, known as *Topological Data Analysis*, or in short as TDA. TDA has its roots in the pioneering works of Robins [14], Edelsbrunner et al. [15] and Zomorodian and Carlsson [16] in persistent homology and became popular with the publication of a landmark paper by Carlsson [17]. Since this paper was published, it has become ubiquitous in data science, with many applications in biology (see, for example, the review mentioned above [13] and the references therein illustrating applications in

structural biology, evolution, cellular architecture and neurobiology). TDA is particularly useful when the data are represented in the form of a graph or network. As such, it proceeds by connecting data points to form a geometric complex structure whose topological behaviour is then used to analyse the data. Returning to the fact that the shape is data, a shape can be characterised through TDA using, for example, the Euler characteristic transform to study the morphology of barley seeds [18], or the persistent homology transform to study the morphology of heel bones of primates [19].

In this paper, we introduce a new method for analysing the morphology of a cell that falls into the second category described above, namely with the cell represented with its contour with an additional point C , taken to be the centre of mass of the cell nucleus. From TDA, we use *persistent homology* to obtain a summary of the morphological features of the cell contour. We use the persistence of sub-level sets of the radial distance function from C and compute the corresponding persistence diagram (see the next section for a primer on persistent homology applied to analysing cell contours). As the contour of each cell is a closed, non-self-intersecting curve, we know that it consists of a single connected component and a single 1-cycle. These two cycles correspond to a persistent cycle with infinite life (called *essential cycles*) in dimensions 0 and 1, respectively. We combine the information from these two persistent cycles by pairing the birth of the essential connected component with the birth of the essential 1-cycle. A pair of cells is then compared by computing the *2-Wasserstein distance* between their *persistence diagrams*, providing a measure of similarity between the two cells. We can then apply various clustering techniques to these similarity scores, to identify homogeneous populations of cells.

The paper is organised as follows. The next section (Section 2) introduces the concept of persistence homology (section 2.1) applied to analysing the morphology of a cell, the construction of the persistence diagram of a cell contour (section 2.2), and the computation of the Wasserstein distance between two persistence diagrams (section 2.4). The Materials and Methods section (section 3) gives information on the experimental data and implementations of the methods mentioned above. The Results section (section 4) discusses the applications of this new method on two systems, hMSCs (section 4.1) that are expected to include sub-populations and, in contrast, HeLa cells (section 4.2) whose morphologies are expected to vary continuously due to local conditions. We conclude with a discussion (section 5) of how to integrate persistent homology with other more traditional techniques for comparing cell shapes.

2 Theory: persistence homology applied to analysing cell contours

2.1 Persistent Homology on Contours

Given a microscopy image of a fixed and immuno-stained cell, we use a graph G to represent the boundary in 2 dimensions. This graph is a list of ordered vertices (pixel locations), V , with edges, E , between neighbouring vertices. Note that G is connected and that every vertex has degree 2, so G consists of precisely one 1-cycle. We extract morphological information using the persistence of connected components of the sub-level sets of a radial function from the centroid of the nucleus.

For a graph G , we say that two vertices v_1, v_2 are in the same *equivalence class*, or *connected component*, if there is a path γ from v_1 to v_2 . For each connected component of G , we choose a representative vertex v and denote the set of vertices v' connected to v by $[v]$. We call the set $\{[v] \text{ for } v \in G\}$ the *connected components* of G .

To use persistent homology, we need to define a filtration on G .

Definition 1 (Sub-level sets and sequence of graphs). *Let f be a function from the vertices V of a graph G to \mathbb{R} , and fix $a \in \mathbb{R}$. The sublevel set $G_a := f^{-1}((-\infty, a])$ is the sub-graph consisting of the set V_a of vertices v with $f(v) \leq a$ and the set of edges E_a between any pair of neighbouring vertices that are both in V_a . Note that for any*

$$a \leq b \in \mathbb{R}$$

we have

$$f^{-1}((-\infty, a]) \subseteq f^{-1}((-\infty, b]),$$

and the sub-level sets form a sequence of nested graphs.

2.2 Persistence Diagrams

Given a nested sequence of graphs $G_0 \subseteq G_1 \subseteq \dots \subseteq G_\alpha$ (in general $G_\alpha = G$ the full graph), we can track the changes in the connected components of the graphs as the filtering parameter varies. Consider some G_β , and let $C_\beta := \left\{ [v_j]^\beta \right\}_{j=1}^{n_i}$ be the set of connected components in G_β . For each connected component of G_β we choose a canonical representative vertex, namely the vertex with the lowest function value. We say that a connected component $[v_j]$ is *born* at time β if there is no vertex v_k in the connected component $[v_j]$ such that v_k is in $C_{\beta-1}$. We say $[v_j]$ *dies* in γ if in G_γ , $[v_j]$ becomes a path connected to a component born before v_j . For any pair $\beta \leq \gamma$ we obtain a map $\mathfrak{A}_\beta^\gamma : C_\beta \rightarrow C_\gamma$, which is induced by the inclusion $\iota_\beta^\gamma : G_\beta \rightarrow G_\gamma$.

Remark 1. The map $\mathfrak{A}_\beta^\gamma : C_\beta \rightarrow C_\gamma$ is obtained from the inclusion $\iota_\beta^\gamma : G_\beta \rightarrow G_\gamma$ by

$$\mathfrak{A}_\beta^\gamma([v]) := \left[\iota_\beta^\gamma(v) \right],$$

which is a well-defined map.

The births and deaths of the connected components can be visualised in a *persistence diagram*.

Definition 2 (dimension 0 Persistence Diagram). *Let f be a function from a graph G to \mathbb{R} , and let $\mathfrak{G} = \{G_a\}_{a \in \mathbb{R}}$. Let $C = \bigcup_{a \in \mathbb{R}} C_a$ be the set of connected components across the sequence of graphs \mathfrak{G} . The dimension 0 persistence diagram, $\mathfrak{D}(\mathfrak{G})$ of \mathfrak{G} is the multi-set of points $(b_j, d_j) \in \mathbb{R}^2$, where b_j is the birth time of $[v_j] \in C$, and d_j its death time. A point with $d_j = \infty$ is called an essential point, and the corresponding equivalence class an essential class.*

Remark 2. Here, we have only defined the persistence diagram in dimension 0. It can be defined analogously for in dimension n by replacing connected components with n -cycles.

We can also define these filtrations and persistence diagrams algebraically, including persistence modules, as in [20].

2.3 Illustration on a simple cell contour

The *input contour* C (see Figure 2A), with the centre of the nucleus marked, forms a graph. Using the centre as a reference point, we construct a *radial distance function* to the graph as follows: for vertices, we use the standard Euclidean distance to the centre of the nucleus, and for edges, we take the maximum of the distances of their two endpoints. Vertices and edges whose radial distances are below a certain threshold (or ‘time step’), form a sub-graph of C (Figure 2B). The *persistence diagram* (Figure 2D),

captures the changes in the connected components of the sequence or filtration of sub-graphs of C obtained at increasing time values.

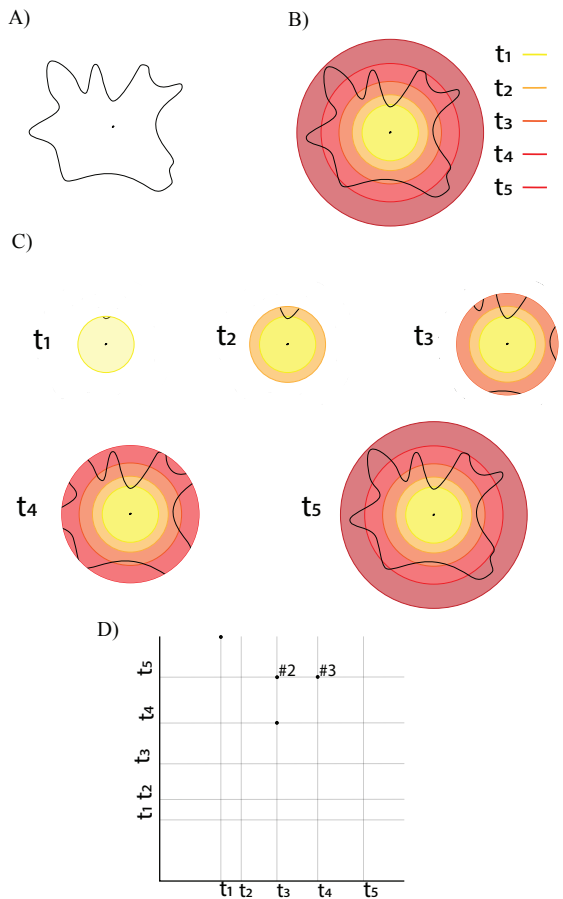


Fig 2. A) *The input data:* a cell contour and the centre of its nucleus marked; the latter serves as the base point for the radial distance function. B) *The radial distance function:* The complete cell contour forms a graph G . The edges of this graph are measured relative to the cell centre by computing the largest Euclidean distance between the centre and the endpoints of the edge: the corresponding measure is the radial distance function with respect to the centre. Edges whose radial distance function is below a given cut-off value (or ‘time step’), illustrated as concentric circles around the centre, define a sub-graph of the whole contour. C) *Graph filtration:* Examples of sub-graphs for five different time steps. The different graphs obtained at increasing values of time form a filtration of the graph G . D) *The persistence diagram* captures the topological properties of the graph filtration. The points marked as ‘#2’ and ‘#3’ indicate that the corresponding points have multiplicity 2 and 3, respectively, in the persistence diagram.

Remark 3. The definition of sub-level sets (definition 1) is cell-wise constant, rather than piecewise-linear one. The distance of a point on an edge from the centre of the function is not the standard Euclidean distance in \mathbb{R}^2 , but rather the maximum of the distances of the two vertices. This is not an issue, as the difference in these two values is bounded, and does not change the topological information we obtain.

The relationship between the sequence of sub-graphs and the persistence diagram is as follows. At t_1 , we see the birth of a single connected component, which has infinite

life and corresponds to the point (t_1, ∞) in the diagram (where ∞ is represented by being at the top of the diagram). At t_2 , there are no changes (no birth or death events). At t_3 , 3 connected components are born. At t_4 , a component born at t_3 merges with another component (and hence dies), which corresponds to the point (t_3, t_4) . We also see the birth of 3 components. At t_5 , we have a single connected component, formed by the remaining 2 components born at t_3 merging with the component born at t_1 , corresponding to the multiplicity 2 point (t_3, t_5) , and all 3 components born at t_4 merge with the original component as well, corresponding to the multiplicity 3 point (t_4, t_5) .

As a multi-set of points, the persistence diagram is

$$\mathcal{D} = \{(t_1, \infty), (t_3, t_4), (t_3, t_5), (t_3, t_5), (t_4, t_5), (t_4, t_5), (t_4, t_5)\},$$

and, since we are only considering the connected components, we call this a *dimension 0* persistence diagram.

As we are using graphs to represent each contour, we can also consider the information captured by the cycles in the sub-graph filtration. Each contour is a simple, closed curve in \mathbb{R}^2 , and hence the corresponding graph G contains a single cycle. Furthermore, this cycle appears only in the filtration when the *last* vertex appears. While it is an important descriptor of the *size* of the contour, it is inefficient to capture this information in a *dimension 1* persistence diagram. Hence, we modify our dimension 0 diagram as follows, so that we capture this information: we pair the birth of the essential class in dimension 0 with the birth of the essential class in dimension 1. In this case, the set of points in the persistence diagram becomes

$$\mathcal{D} = \{(t_1, t_5), (t_3, t_4), (t_3, t_5), (t_3, t_5), (t_4, t_5), (t_4, t_5), (t_4, t_5)\}.$$

Remark 4. Readers familiar with persistent homology and persistence diagrams will notice that this is a non-standard modification. Due to the nature of the contours, performing this *essential pairing* allows us to more efficiently represent and compare the topological descriptors.

2.4 Comparing two persistence diagrams using the Wasserstein distance

A persistence diagram provides a summary of the changes in the connected components as we progress along the sequence of graphs. Consider two sequences of graphs

$$\mathfrak{G}^1 = G_0^1 \rightarrow G_1^1 \rightarrow \dots G_{\alpha_1}^1$$

and

$$\mathfrak{G}^2 = G_0^2 \rightarrow G_1^2 \rightarrow \dots G_{\alpha_2}^2,$$

corresponding to two cell contours, with their associated persistence diagrams $D_1 = \mathfrak{D}(\mathfrak{G}^1)$, $D_2 = \mathfrak{D}(\mathfrak{G}^2)$. We define the distance between the cell contours as the distance between D_1 and D_2 , where the distance is the *Wasserstein distance*, defined below.

Imagine that there are N farms that serve N markets, and assume balance, that is, that each farm produces enough fruits and vegetables as needed by one market. A company in charge of the distribution of the produce from the farms to the market will take into account the individual cost of transport from any farm to any market to find an “optimal transportation plan”, namely an assignment of farms to markets that leads to a minimal total cost for the transport. The seemingly simple problem can be traced

back to the work of Monge in the 1780s [21]. What makes it so interesting is that its solution includes two essential components. First, it defines the assignment between farms and markets, enabling the registration between those two sets. Second, and more relevant to us, it defines a distance between the set of farms and the set of markets, with such a distance being referred to as the Monge distance, the Wasserstein distance, or the earth mover’s distance, depending on the field of applications. Formally, if F is the set of farms and M the set of markets, and if we define $C(i, j)$ the cost of transport between farm i and market j , the assignment problem refers to finding a bijection f between F and M that minimises

$$U = \sum_{i \in F} C(i, f(i)). \quad (1)$$

Note that f can be seen as a permutation of $\{1, \dots, N\}$. As mentioned above, the optimal U_{min} is a distance between F and M . This is the distance that we use to compare two cell contours on the basis of their persistence diagram.

As described above, a persistence diagram is defined by a set of points. Let S_1 (resp. S_2) be the set of points associated with D_1 (resp. D_2):

$$\begin{aligned} S_1 &= \{X_1, \dots, X_N\} \\ S_2 &= \{Y_1, \dots, Y_N\} \end{aligned}$$

We define the cost matrix C as a power of the Euclidean distance, that is,

$$C(X_i, Y_j) = \|X_i - Y_j\|^p$$

The p -Wasserstein distance between S_1 and S_2 is then:

$$W_p(S_1, S_2) = \left(\min_f \sum_{x_i \in S_1} \|X_i - f(X_i)\|^p \right)^{1/p}$$

The formalism defined above assumes that the two sets of points S_1 and S_2 considered have the same size, that is, there are as many points in D_1 as there are points in D_2 . There is no reason why this is the case. In the more general case, S_1 contains N_1 points and S_2 contains N_2 , with $N_1 > N_2$, without loss of generality. This problem, however, can easily be reduced to the balanced case presented above by adding $N_1 - N_2$ pseudo, or “ghost” points in S_2 that the two corresponding sets have the same cardinality. The distance between a point in S_1 and one of these pseudo-points can be chosen arbitrarily. One option is to position the “ghost” points on the diagonal of D_2 .

In the following, we will use the 2-Wasserstein distance to compare two cell contours via their persistence diagrams.

3 Materials and Methods

3.1 Human Mesenchymal Stem Cells

Adult human mesenchymal stem cells (hMSCs) were purchased from Lonza (#PT – 2501 Basel, Switzerland) and cultured in low glucose DMEM (Gibco, #1885 – 023) supplemented with 10% FBS (Sigma-Aldrich, Ref. F7524), and 1% penicillin/streptomycin (Gibco, #15140122) in regular tissue culture treated flasks (greiner Bio-One, 75cm², #658175) at 37° C and 5.0% CO₂. Cells were kept subconfluent at low density all the time and passaged and split every two or three days

using pre-warmed trypsin / EDTA (0.25%) (Sigma-Aldrich T4049) for an incubation time of 3 min after a washing step with buffered phosphate saline (PBS) (Gibco, #14190144). Cells were seeded on ibidi μ -Dishes (35 mm, high, ibiTreat, Cat.No: #81156) at a density of 500 cells cm^{-1} to maintain a sufficient number of isolated cells for observation and grown for 24 hours under identical culture conditions. The cells were then washed once with PBS and chemically fixed for 5min in a 10% solution of formaldehyde (Sigma-Aldrich, 252549) in PBS. The cells were then permeabilized with TritonX (Sigma-Aldrich, T 9284) and extensively washed with PBS.

3.2 HeLa cells

HeLa cells (Leibniz Institute, DSMZ, ACC 57, RRID:CVCL.0030) were cultured in Dulbecco's Modified Eagle's Medium (DMEM, Sigma-Aldrich D5671) supplemented with 10% fetal bovine serum (Sigma-Aldrich F7524), 5% sodium pyruvate solution (Sigma-Aldrich S8636) and 5% penicillin/streptomycin (Sigma-Aldrich P4333). Cells were grown in T-25 flasks (BioLite No. 130189 Thermo Scientific, Germany) at 5% CO_2 at 37°C. Cells were split at 80% confluence every two to three days using pre-warmed trypsin / EDTA (0.25%) (Sigma-Aldrich T4049) incubation of 3 minutes for detachment up to a maximum of 20 passages per cell batch.

Briefly, 25 mm round coverslips were treated with 0.03 N NaOH solution at 90°C for 30 minutes. The treated coverslips were coated with 3-aminopropyltriethoxysilane (APTES, Sigma-Aldrich, 440140) for 5 minutes followed by washing steps with PBS. The coverslips were then incubated with the solution of 0.5% glutaraldehyde (Sigma-Aldrich, G7651) for 30 minutes and extensively washed with PBS. The coverslips were then treated with 0.4 mM sulfo-SANPAH (Thermo Scientific 22589-50MG) solubilised in 50 mM HEPES buffer at a pH of 8.0. Subsequently, the treated coverslips were placed under a UV lamp at a wavelength of 365 nm for 15 minutes for cross-linker activation, followed by washing with HEPES solution. After this, the coverslips were coated with 50 $\mu\text{g}/\text{ml}$ concentration fibronectin (Gibco, 33010018) overnight at room temperature.

HeLa cells were seeded at a density of 5000 cells per well in a 6 well plate. After 24 hours, the cells were fixed in paraformaldehyde (PFA) 4% (m/V) after 24 hours. The cells were then permeabilized with 0.5% (V/V) Triton for 15 minutes and blocked for 30 minutes with 1% bovine serum albumin (BSA) in PBS.

Actin was stained with fluorescently labelled phalloidin Atto 550 (Atto Tec AD 550-81) for 15 minutes, followed by washing with PBS. The nucleus was stained with Hoechst 33342 (Invitrogen H3570).

3.3 Fluorescence Staining of Cells

Both cell samples were fluorescently stained to reliably quantify the contours of the cell and the nucleus after fixation. Filamentous actin was stained using fluorescent Phalloidin-Atto 550 (ATTO-TEC GmbH, AD 550 – 81) to quantify its contour and the nucleus was visualised using the DNA selective Hoechst dye (Invitrogen, Hoechst #33342).

3.4 Unbiased Microscopy

The fixed hMSCs were imaged on an inverted fluorescence microscope (Zeiss AxioObserver, Oberkochen, Germany) using a 20x objective (Zeiss, Plan-Neofluar, 440340-9904) and recorded by a sCMOS camera (Andor Zyla, 4.2P USB3.0) using two filter sets (blue emission (Zeiss Filterset 49) and red emission (AHF, F46-008)) for the stained nucleus and actin, respectively. Since the cellular outline is the major morphological parameter we wanted to assess, we ensured unbiased data acquisition of

the samples by inspecting using the nucleus fluorescence channel first and only selecting cells that were isolated (no other nucleus in the field of view) and had a healthy-looking non-deformed nucleus. Multiple nuclei, ill-shaped nuclei, as well as any oddly shaped nuclei were excluded to avoid recording cell outlines from abnormal cells. Subsequently, the actin channel of the cell was recorded to complete the data set for each cell.

HeLa cells were imaged on the same inverted fluorescence microscope after fixation using a 40x objective (Zeiss, LD Achromplan, 440865) and an Andor Sona-4BV6X sCMOS camera.

3.5 Image Processing and Contour Generation

We used the FilamentSensor2.0 tool [22] to perform image processing and extract the contour of each cell from the actin image. Here, we used the feature “Include Area-Outline” to export the contour from the binarised image of the cells. The *centre* of the cell is obtained from the *centre of mass* from the aligned microscopy image of the nucleus, where we thresholded the nucleus in Fiji [23] using the “Otsu” method, before outlining it and determining the x - and y -coordinates of the centre of mass.

3.6 Contour Analysis: computing the distance between 2 cells

After extracting the contour from each image and identifying the centre of the nucleus, we convert it to the graph representation G . Recall that every vertex in G is of degree 2, and G contains a single cycle. Let $V = \{v_i\}_{i=1}^n$ be the set of vertices of G , ordered clockwise around the contour. Then every edge e of G is of the form (v_i, v_{i+1}) , where $v_{n+1} = v_1$. Before we obtain our sequence of graphs \mathfrak{G} , we *clean* our graph representation G of C by replacing any set of consecutive edges $\{(v_i, v_{i+1}), \dots, (v_{j-1}, v_j)\}$ which are co-linear (having the same x or y coordinate) with the edge (v_i, v_j) and removing the vertices v_k for $i < k < j$.

Remark 5. Consider a contour C , and let G be the original graph representation and G' the graph after it has been cleaned. As the metrics on the edges of G, G' are defined as the maximum of the values at the 2 vertices, the sequences of graphs \mathfrak{G} and \mathfrak{G}' generated by these metrics on G and G' , respectively, will have different topological features. In particular, connected components may be born *later*, by the removal of vertices that are closer to the base point of the radial distance function. These changes in values are bounded and therefore, by the stability of persistence diagrams [24], the distance between the respective persistence diagrams is also bounded. Although it is possible to generate contours where this cleaning process leads to large bounds on the distance between the persistence diagrams, the geometric features that lead to this are not of concern in our application. Hence, we prioritise computational efficiency and proceed with the cleaned graphs.

Working with the cleaned graph G_X for each cell X , we filter G_X (see Definition 1 and Section 2.3), and obtain a persistence diagram D_X (Definition 2). Then we construct a distance matrix M , using the 2-Wasserstein distance between the persistence diagrams D_X, D_Y as the distance between two cells X, Y .

3.7 Clustering cells based on their contour

Clustering is the task of regrouping cells such that those that belong to the same group, referred to as a cluster, are more similar to each other than to those in other clusters. We use the 2-Wasserstein distance between the corresponding persistence diagrams as the *similarity* score between a pair of cells, see Section 2.4. The clustering of the cells is then performed using the agglomerative hierarchical clustering analysis, or HCA. The is

a bottom-up approach in which each cell starts in its own cluster, and pairs of clusters are merged iteratively until all cells belong to the same cluster. The whole procedure defines a clustering tree. Although the distance between two cells is clearly defined above, a key element is to define the distance between two clusters. When two clusters A and B are sets of elements, the distance between A and B is then defined as a function of the pairwise distances between their elements. Four common choices of linkage are:

- **Average linkage:** the distance between two clusters is the arithmetic mean of all the distances between the objects of one and the objects of the other:

$$d(A, B) = \sum_{a \in A} \sum_{b \in B} \frac{d(a, b)}{|A||B|}$$

where $|\cdot|$ stands for cardinality. Average linkage, also called UPGMA, is the default linkage for most HCA implementations.

- **Single linkage:** the distance between two clusters is the smallest distance between the objects in one and the objects in the other.

$$d(A, B) = \min\{d(a, b), a \in A, b \in B\}$$

- **Complete linkage:** the distance between two clusters is the largest distance between the objects in one and the objects in the other.

$$d(A, B) = \max\{d(a, b), a \in A, b \in B\}$$

- **Ward's linkage** accounts for the variances of the clusters to be compared. For a cluster A , the variance $SSE(A)$ is defined as:

$$SSE(A) = \sum_{a \in A} d(a, m(A))^2$$

where d is the underlying distance used to compare two objects and $m(A)$ is either the centroid (if it can be computed) or mediod of the cluster (the mediod is the point in A that has the least total distance to the other points in A). The Ward distance between two clusters A and B is then:

$$d(A, B) = SSE(A \cup B) - (SSE(A) + SSE(B))$$

The choice of the linkage can have a significant influence in the clustering found by HCA: for example, simple linkage only looks locally at cluster distance, and as such may lead to elongated clusters, while reversely complete linkage will have a tendency to generate more compact clusters. There is no consensus as to which linkage scheme to use for a specific data set; this is, in fact, an active area of research.

To avoid possible biases associated with the choice of linkage, we will use all four options in our analyses, performing HCA with [25]. However, this requires a way to compare the results of one option with those of the others. We chose our own concept of purity to perform such a comparison, which is defined as follows. Let C_1 be one cluster identified with HCA with a linkage method L_1 . It is possible that C_1 may not be identified as its own cluster within the tree T_2 generated with another linkage method L_2 . To assess how well T_2 recognises C_1 , we follow the following algorithm:

- 1) First, we choose a seed, S_1 , i.e. an object that belongs to C_1 . We initialise a list of objects $O = \{S_1\}$.

- 2) We identify the leaf of T_2 corresponding to S_1 , and add to the list O the object that has the same parent P_1 in T_2 as S_1 .
- 3) We find the parent P_2 of P_1 and add to O all objects that are in the sub-tree of T_2 starting from P_2 . We then set $P_1 \leftarrow P_2$.
- 4) We repeat step 3 until O contains all objects in C_1

If the results with the linkage L_2 match exactly the results with the linkage L_1 , O will be equal to C_1 . However, in general, O will be bigger because it will include objects that are found by L_2 to be similar to objects in C_1 that were not identified by L_1 . The *purity* $P(C_1/L_2)$ of C_1 with respect to L_2 is then defined as:

$$P(C_1/L_2) = \frac{N - |O|}{N - |C_1|} \quad (2)$$

where $|\cdot|$ stands for cardinality and N is the total number of objects. Note that P is between 0 and 1. The closer P is to one, the more consistent the two linkage strategies L_1 and L_2 are with respect to C_1 .

4 Results and discussion

In this section, we report how our method for comparing the shapes of cells can be used to identify unusual cells (i.e., outliers) and subpopulations within a cell population. We consider both human mesenchymal stem cells (hMSCs) and HeLa cells. HeLa cells are a long-established, immortalised cancer cell line. They are a commonly used cell line for culturing in *in vitro* conditions, showing relatively consistent growth patterns and morphologies within a population, despite some heterogeneity. hMSCs are primary cells, on the other hand, derived from bone marrow directly from patients. They are not immortalised or further altered and exhibit an inherent natural heterogeneity, both in morphology and function, due to their preparation and selection method.

We analyse a population of hMSCs, $X1$ (Section 4.1) and a population of HeLa cells, $Y1$ (Section 4.2), with the experimental setup and analysis pipeline described in Section 3.

4.1 $X1$: sub-populations of hMSCs

The set $X1$ consists of 140 cells. These cells have already been selected based on manual inspection, as described in Section 3.4. To further analyse the homogeneity of this set of cells, we computed all pairwise distances between the cell contours using the persistence homology technique described above. The corresponding distance matrix is visualised as a heat map in Figure 3. The column/row of mostly bright yellow suggests that there is one cell that differs significantly from the others. This cell is shown in Figure 4. Clearly, this cell is oddly shaped: it is long and thin, with three long filipods, significantly different from the expected shape of an hMSC (see Figure 1 and Figure 6). Such a shape is usually considered an outlier.

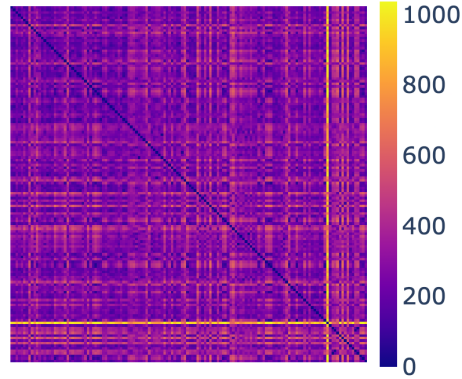


Fig 3. Heat map of the distance matrix for $X1$. There is a cell that has distinctly higher than average distances to the other cells, indicated by the row/column of mostly bright yellow. Generated with [26].

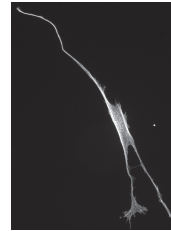


Fig 4. Image of the unusual cell shape ($X1-015$) identified in Figure 3 (image processed using [27].)

We perform clustering of cell contours in $X1$ using the Wasserstein distance between their associated persistence diagram, in the presence (Figure 5), and the clustering in the absence of the ‘outlier’ $X1-015$ identified above is obtained by removing the single leaf branch on the right side of each dendrogram. We used HCA with four different linkages: average, complete, single, and Ward.

As expected, cell $X1-015$ is identified as its own cluster with all four linkages in Figure 5 (it is the cell found at the extreme right of all four dendrograms). This cell has a unique shape that differentiates it from other hMSC cells. Although there are many possible reasons for this behaviour, $X1-015$ is considered an outlier.

The clustering of the set $X1$ without the outlier $X1-015$, identifies subgroups. We obtain the dendrograms for $X1$ without $X1-015$ by removing the singleton cluster in black which corresponds to $X1-015$. Those subgroups appear to differ under different choices of HCA linkage (Figure 5). This behaviour is not unexpected, as different linkage schemes capture different geometries for the cluster (see Section 3.7). It is common to focus on only one linkage scheme, usually the average linkage, and ignore the others. Our approach is different. We use all four linkages and assess their consistency, as illustrated in Figure 5. We start with the average linkage scheme and cut the associated dendrogram to obtain four clusters. These four clusters are referenced as A (red, 86 elements), B (blue, 7 elements), C (green, 22 elements), and D (purple, 24 elements). We then consistently colour the dendrograms for all linkage schemes based on those clusters A, B, C, and D. As expected, there are differences. However, some



Fig 5. Dendrograms for $X1$, the colours correspond to 4 clusters obtained using average linkage. (A) Average linkage. (B) Complete linkage. (C) Single linkage. (D) Ward linkage. In each of these, there is an outlier, with the corresponding leaf coloured purple. Generated with [28].

consistencies are observed. For example, we note that cluster D (in purple) is grouped together across all 4 linkage schemes. To confirm this visual consistency, we computed a purity score (see Section 3.7) of the clusters obtained with the average linkage in all four linkage schemes. The purity score quantifies how “pure” a group of objects is within a dendrogram. It is computed by first identifying the subtree within the dendrogram that contains all objects within that group. If this subtree only contains this group, it is deemed pure and the purity score is set to 1. If, instead, this subtree contains other objects, its purity is reduced. When the subtree is the whole tree, the purity score is reduced to 0. The purity scores of clusters A to D are reported in Table 1, while examples of cells for each clusters are shown in Figure 6.

Linkage	Cluster			
	A (red, $n = 86$)	B (blue, $n = 7$)	C (green, $n = 22$)	D (purple, $n = 24$)
average	1.0	1.0	1.0	1.0
complete	0.0	1.0	0.732	1.0
single	0.021	0.0	0.056	1.0
ward	0.0	1.0	0.690	1.0

Table 1. Purity score of the 4 clusters obtained with the average linkage for $X1$ without $X1-015$, see Figure 5. The colour and size of each cluster is in parentheses.

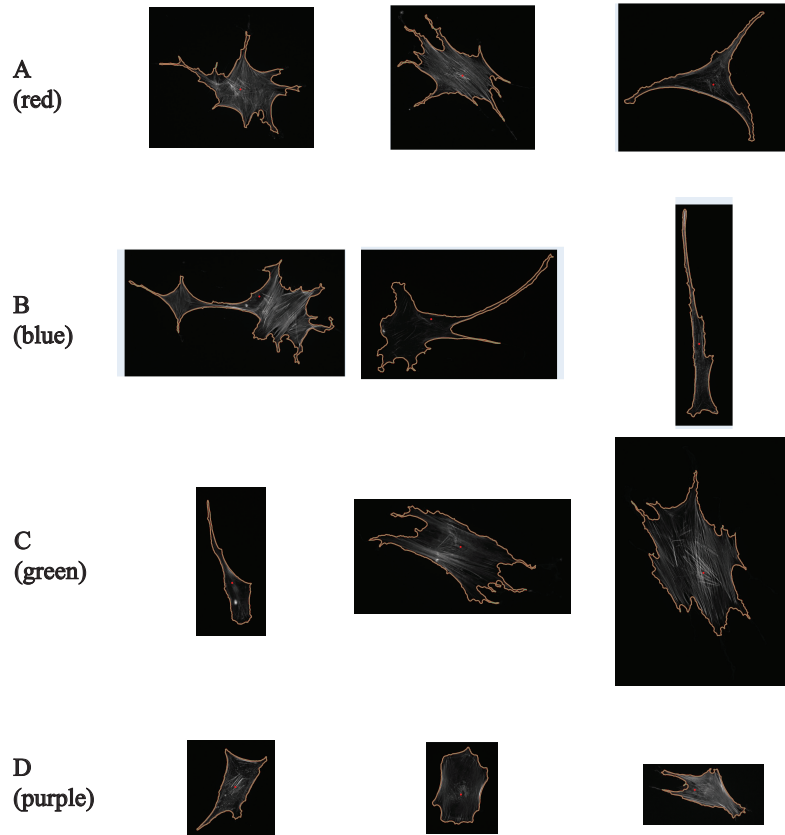


Fig 6. Example cells from each cluster of the set $X1$ without $X1-015$. Those clusters are identified with HCA and average linkage scheme (see Figure 5). All cell images are shown at the same magnification level. Images were processed using [27].

As mentioned above, cluster D (purple) is visually homogeneous within all four linkage schemes: this is confirmed as its purity scores remain equal to 1. The cells in this cluster have compact shapes and a prominent nucleus, as expected from cells that have been plated on glass. The same types of cells were distinguished as a sub-population FC by Haaster *et al.* [29]. In contrast, cluster A (red) is much less consistent within the different linkage schemes, with purity scores close to 0 (with the obvious exception of the average linkage). Visually, cells belonging to cluster A are more heterogeneous, with a star-shaped or a triangular shape (first row of Figure 6). This group of cells maps with the sub-population RS identified by Haaster *et al.* Cells belonging to cluster B are significantly more elongated. Their purity score is high with the exception of the single linkage scheme, but this could just be anecdotal as there are only 7 cells in this cluster. They may correspond to spindle-shaped elongated cells, fibroblastic in shape, identified as SS cells by Haaster *et al.* The cells in cluster C are mostly compact, similar to those in cluster D, but usually larger. The purity scores of cluster C are close to 1, indicating that they form a group with homogeneous shapes. They were probably identified as belonging to the FC subpopulation by Haaster *et al.*

4.2 Y1: heterogeneity of HeLa cell shapes

The set $Y1$ consists of 100 cells. These cells have already been selected based on manual inspection; see Section 3.4. We followed the procedure described in Section 4.1 for the hMSCs to compute all pairwise distances between the cell contours using the methodology of Section 3.6. The corresponding distance matrix is visualised as a heat map in Figure 7. In contrast to the hMSCs for which we identified a clear outlier (see Figure 3), we do not identify HeLa cells that we would unambiguously classify as outliers.

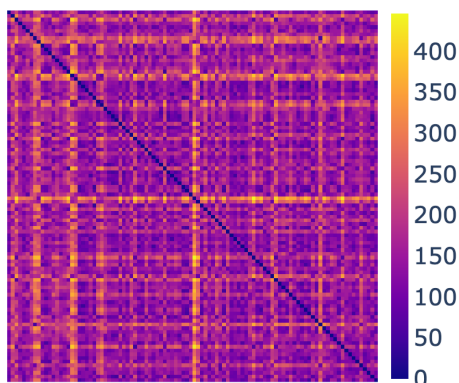


Fig 7. Heat map of the distance matrix for $Y1$. Generated with [26].

We clustered the cell contours in $Y1$ using the Wasserstein distance between their associated persistence diagrams (Figure 8), using the four links from Section 3.7. Similarly to the analysis of $X1$ above, we defined 4 clusters based on the average linkage scheme. These four clusters are referenced as A (red), with 7 elements, B (green with 65 elements, C (cyan, 15 elements) and D (purple, 13 elements). We then consistently colour the dendrograms for all linkage schemes based on those clusters A, B, C, and D. There are no consistencies in these 4 clusters obtained across the four linkages in Figure 8. This is reflected in the purity scores that are not consistent (see Table 2). This likely indicates that the HeLa do not separate into homogenous subpopulations.

In Figure 9, we provide example cells for each of the four clusters obtained using the average linkage, cluster A (in red, $n = 7$ elements), cluster B (in green, $n = 65$ elements), C (in blue, $n = 15$ elements), and D (in purple, $n = 13$ elements). See Figure 9 for plots of the contours with the centre mass of the nucleus marked. HeLa cells in all four clusters visually look homogeneous, with some shape heterogeneity; i.e. with some cells having a more triangular structure, or some a pentagonal layout, and others are slightly more ellipsoidal. These three structures are present in each of the four clusters. Visually, the cells in cluster A are elongated, but there were only 7 cells. In cluster C the cells are more heterogeneous having elongated, triangular, or hexagonal shape. In cluster D the cells are comparatively compact (means have smaller values for cell area), which supports future possibilities of including the morphometric parameters like area and aspect ratio in our topological data analysis approach. Overall, HeLa cells population is homogeneous with variable shapes in each cluster, but no distinct identifiable sub-population present. Considering the purity scores, we see that none for four clusters has a high purity score across all linkage types, suggesting the presence of heterogeneous shapes among the clusters. This is not unexpected, as HeLa cells are a

well established, robust cell line and we imaged cells that all originated from the same cell culture flask at the same time point and identical experimental conditions.

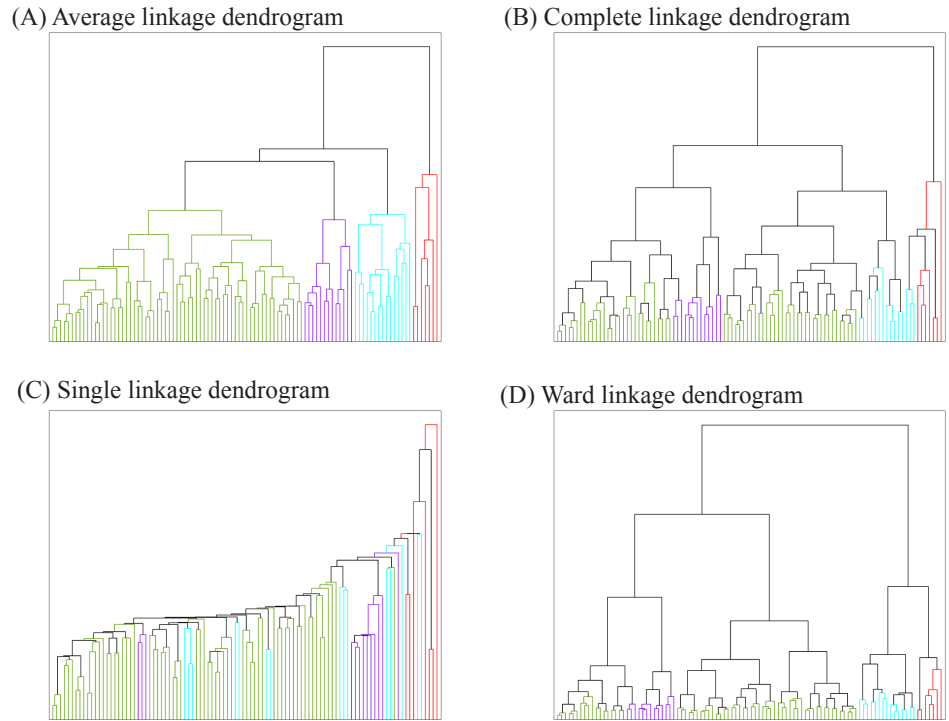


Fig 8. Dendrograms for Y1, the colours correspond to 4 clusters obtained using average linkage. (A) Average linkage. (B) Complete linkage. (C) Single linkage. (D) Ward linkage. In each of these, there is a consistent sub-population, coloured purple. Generated using [28].

Linkage	Cluster			
	A (red, $n = 7$)	B (green, $n = 65$)	C (blue, $n = 15$)	D (purple, $n = 13$)
average	1.000	1.0	1.000	1.000
complete	0.968	0.285	0.000	0.655
single	0.000	0.314	0.047	0.114
ward	1.000	0.629	1.000	0.793

Table 2. Purity score of the 4 clusters obtained with the average linkage for Y1, see Figure 8. The colour and size of each cluster is in parentheses.

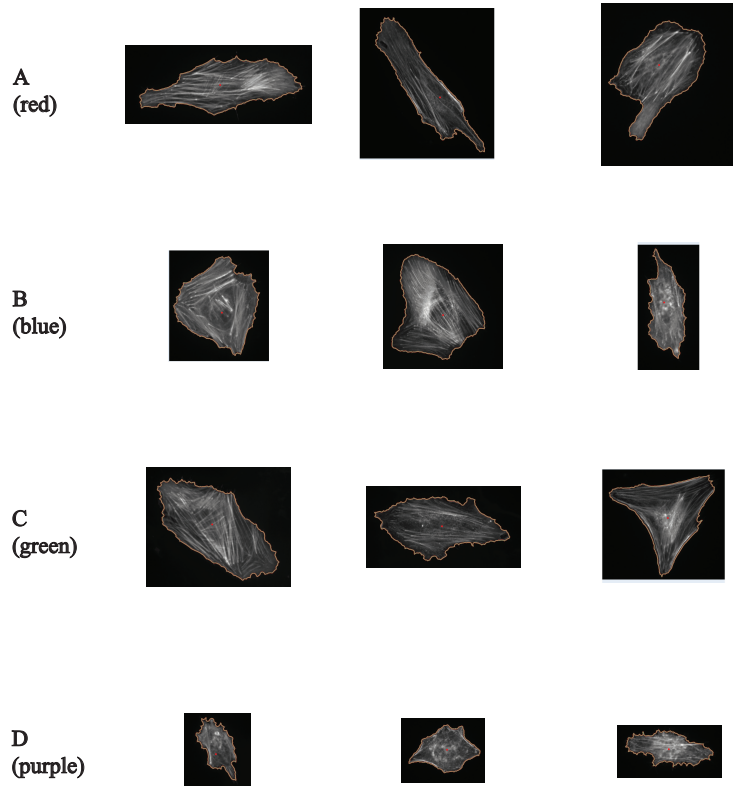


Fig 9. Example cells from each cluster of the set $Y1$. Those clusters are identified with HCA and average linkage scheme (see Figure 8). All cell images are shown at the same magnification level. Images were processed using [27].

4.3 $X1$ vs $Y1$: two different types of variability

The method we have developed follows a simple generic scheme when analysing a population: it computes distances between its members and uses those distances to define sub-groups within the whole population. Interestingly, the two examples described above, namely populations of hMSCs and of HeLa cells exhibit two different behaviours when investigated with our method, which illustrate intrinsic properties of those cell types.

Application of our method on hMSCs identified (at least) four different sub-populations in our sample. hMSCs are primary cells that are harvested from the bone marrow of patients and selected due to well-known surface markers. It is intrinsic to this procedure that hMSCs are a heterogeneous cell population, reflected in varying morphological and biological properties [30–32]. It was established that an hMSC population can be divided into at least three subpopulations with intrinsic characteristics, small rapidly self-renewing cells, spindle-shaped cells, and large, flattened cells [29, 33]. The consistent clustering results found with different HCA strategies is a good indicator of this discrete variability in the hMSC morphology.

In contrast, our clustering results indicate a more continuous variability for the morphology of the specific HeLa cell line. Those are immortalised cancer cells that are

cultured for many passages *in vitro* and have been reported to contain a very large number of genomic variants [34]. A large study across different HeLa batches in many international laboratories identified substantial heterogeneity between HeLa variants [35]. However, for a specific type of this cell line, HeLa cells are expected to maintain a general epithelial-like polygonal morphology as a characteristic of the population (see Figure 9). Heterogeneity is then expected to reflect local environmental conditions, i.e. a continuous variability rather than a discrete set of sub-populations. This is well reflected in the absence of consensus in the different clustering strategies for the Y1 cell sample.

5 Conclusion

Cell biologists commonly study in parallel the morphology of cells with the regulation mechanisms that affect this morphology. In the case of stem cells, for example, the shapes they assumed when plated on a substrate with different rigidities are expected to define the morphological descriptors of mechano-directed differentiation. However, the heterogeneous nature of the cell population is a major difficulty when studying the cell shape based on images from digital microscopes. It is common to manually assess first all the images associated with a population of cells under study in order to identify “outliers”, i.e. cells with unusual shapes that raise questions on their nature (i.e. these cells could be associated with contamination) or on the presence of experimental artefacts. The purpose of the present study was to propose an alternative automated method to help with this manual assessment. We have developed a new method for analysing cell shapes that is based on three elements:

- ***A description of cell shapes using persistence homology.*** The shape of a cell is defined by its contour and the position of its nucleus. We compute a filtration of the edges that define the contour, using the radial distance to the nucleus as a filter. This filtration is used to define a persistence diagram that serves as a signature of the cell contour.
- ***A distance between two cells.*** This distance is the Wasserstein distance between the persistence diagrams of their contours.
- ***A measure of homogeneity of cell subgroups.*** We perform hierarchical clustering on cell shapes using the distance defined above, with four different linkage schemes. We define a purity score for subgroups of cells within the dendrograms associated with the clustering. This purity score reflects homogeneity.

We have tested our method on hMSCs, that are known to be heterogeneous with the presence of well-characterised sub-population, and HeLa cells, whose morphological differences are associated with continuous variability. We have shown that it automatically identifies unusual cells that can then be deemed outliers or not, as well as sub-populations that are consistent with previous analyses of sub-populations of hMSCs [29], and that, in the case of HeLa, confirms the expected homogeneity.

There are many morphometric parameters that could have been included to complement our topological data analysis, such as cell area, aspect ratios, ellipticity, curvature of the contours, and those coming from conformal geometry. It is our intent to complement our analyses with a more comprehensive set of morphological signatures of cell shapes. In addition, all those parameters, including the persistence diagrams presented in this paper, are computed based on 2D images. Cells are 3D objects and should ultimately be studied as such. The concepts we have introduced in this paper extend to the analysis of 3D surfaces. We will explore this in further studies.

Data Availability

All images used in this paper, as well as the code to analyse them, are available on GitHub PDaMSoC-data, which is also archived on Zenodo (10.5281/zenodo.16760103). In the repository, there are 4 directories (X1, X2, X3, Y1) containing data sets, with X1, X2, X3 consisting of populations of hMSCs and Y1 a population of HeLa cells. In this paper, we presented analysis of the datasets X1 and Y1. We did analyse X2 and X3, but did not obtain results that were distinctly different from X1.

Acknowledgments

We thank Stephan Huckemann, Katharine Turner, Benjamin Eltzner, Stephan Tillmann, Fariza Rashid, and Lamiae Azizi for many useful discussions at various stages of this project. FR and PY gratefully acknowledge Matthias Weiss (Experimental Physics I, University of Bayreuth, Germany) for granting access to cell culture and laboratories, as well as funding consumables and the fruitful discussion that contributed to this work. This research was funded in whole or in part by the Austrian Science Fund (FWF) ESP9584724. For open access purposes, the author has applied a CC BY public copyright license to any author-accepted manuscript version arising from this submission.

References

1. Engler AJ, Sen S, Sweeney HL, Discher DE. Matrix Elasticity Directs Stem Cell Lineage Specification. *Cell*. 2006;126(4):677–689. doi:10.1016/j.cell.2006.06.044.
2. Zemel A, Rehfeldt F, Brown AEX, Discher DE, Safran SA. Optimal matrix rigidity for stress-fibre polarization in stem cells. *Nature Physics*. 2010;6(6). doi:10.1038/NPHYS1613.
3. Zemel A, Rehfeldt F, Brown A E X, Discher D E, Safran S A Cell shape, spreading symmetry, and the polarization of stress-fibers in cells. *Journal of Physics: Condensed Matter*, 2010;22(19). doi:10.1088/0953-8984/22/19/194110
4. Costa LA, Eiro N, Fraile M, Gonzalez LO, Saá J, Garcia-Portabella P, et al. Functional heterogeneity of mesenchymal stem cells from natural niches to culture conditions: implications for further clinical uses. *Cellular and Molecular Life Sciences*. 2021;78(2):447–467. doi:10.1007/s00018-020-03600-0
5. Phinney DG. Functional heterogeneity of mesenchymal stem cells: Implications for cell therapy. *Journal of Cellular Biochemistry*. 2012;113(9):2806–2812. doi:10.1002/jcb.24166
6. Chen L, Rottensteiner F, Heipke C. Feature detection and description for image matching: from hand-crafted design to deep learning. *Geo-spatial Information Science*. 2021;24(1):58–74. doi:10.1080/10095020.2020.1843376
7. Zhou SK, Greenspan H, Davatzikos C, Duncan JS, Van Ginneken B, Madabhushi A, et al. A Review of Deep Learning in Medical Imaging: Imaging Traits, Technology Trends, Case Studies With Progress Highlights, and Future Promises. *Proceedings of the IEEE*. 2021;109(5):820–838. doi:10.1109/JPROC.2021.3054390
8. Alt H. 16. The Computational Geometry of Comparing Shapes. In: Albers, S., Alt, H., Näher, S. (eds) *Efficient Algorithms*. Lecture Notes in Computer Science. Springer Berlin Heidelberg; 2009:235–248. doi:10.1007/978-3-642-03456-5_16

9. Gorelick L, Galun M, Sharon E, Basri R, Brandt A. Shape Representation and Classification Using the Poisson Equation. *IEEE Transactions on Pattern Analysis and Machine Intelligence*. 2006;28(12):1991–2005. doi:10.1109/TPAMI.2006.253
10. Manay S, Cremers D, Hong BW, Yezzi AJ, Soatto S. 6. Integral Invariants for Shape Matching. In: Krim, H., Yezzi, A. (eds) *Statistics and Analysis of Shapes. Modeling and Simulation in Science, Engineering and Technology*. Birkhäuser Boston. 2006:137-166. doi:10.1007/0-8176-4481-4_6
11. Bauer M, Bruveris M, Michor PW. Overview of the geometries of shape spaces and diffeomorphism groups. *J Math Imaging and Vis*. 2014;50:60–97. doi:10.1007/s10851-013-0490-z
12. Dogan G, Bernal J, Hagwood CR. A Fast Algorithm for Elastic Shape Distances Between Closed Planar Curves. In: *Proceedings of the IEEE Conference on Computer Vision and Pattern Recognition (CVPR)*; 2015:4222–4230. doi:10.1109/CVPR.2015.7299050
13. Amézquita EJ, Quigley MY, Ophelders T, Munch E, Chitwood DH. The shape of things to come: Topological data analysis and biology, from molecules to organisms. *Developmental Dynamics*. 2020;249(7):816–833. doi:10.1002/dvdy.175
14. Robins V. *Computational Topology at Multiple Resolutions: Foundations and Applications to Fractals and Dynamics*. University of Colorado; 2000.
15. Edelsbrunner H, Letscher D, Zomorodian A. Topological persistence and simplification. *Discrete & Computational Geometry*. 2002;28:511–533. doi:10.1007/s00454-002-2885-2
16. Zomorodian A, Carlsson G. Computing persistent homology. In: *Proceedings of the twentieth annual symposium on Computational geometry*; 2004. p. 347–356.
17. Carlsson G. Topology and data. *Bulletin of the American Mathematical Society*. 2009;46:255–308.
18. Amezquita E, Quigley M, Ophelders T, Landis JB, Koenig D, Munch E, et al. Measuring hidden phenotype: quantifying the shape of barley seeds using the Euler characteristic transform. *in silico Plants*. 2022;4(1). doi:10.1093/insilicoplants/diab033
19. K. Turner, S. Mukherjee and D. M. Boyer Persistent homology transform for modeling shapes and surfaces *Information and Inference: A Journal of the IMA*. 2014;3(4):310-344. doi:10.1093/imaiai/iau011
20. Chazal F, de Silva V, Glisse M, Oudot S. *The Structure and Stability of Persistence Modules*. Springer Briefs in Mathematics. 2016. doi:10.1007/978-3-319-42545-0
21. Monge G. Mémoire sur la théorie des déblais et des remblais. *Histoire de l'Académie Royale des Sciences et Mémoires de Mathématique et de Physique tirés des registres de cette Académie*. 1781;1784:666–704.
22. Hauke L, Primeßnig A, Eltzner B, Radwitz J, Huckemann SF, Rehfeldt F. FilamentSensor 2.0: An open-source modular toolbox for 2D/3D cytoskeletal filament tracking. *PLOS ONE*. 2023;18(2):e0279336. doi:10.1371/journal.pone.0279336

23. Schindelin J, Arganda-Carreras I, Frise E, Kaynig V, Longair M, Pietzsch T, et al. Fiji: an open-source platform for biological-image analysis. *Nature Methods*. 2012;9(7):676–682. doi:10.1038/nmeth.2019
24. Skraba P, Turner K. Wasserstein Stability for Persistence Diagrams. *arXiv: Algebraic Topology*. 2020. doi:10.48550/arXiv.2006.16824
25. Pedregosa F, Varoquaux G, Gramfort A, Michel V, Thirion B, Grisel O, et al. Scikit-learn: Machine Learning in Python. *Journal of Machine Learning Research*. 2011;12:2825–2830.
26. Inc PT. Collaborative data science; 2015. Available from: <https://plot.ly>.
27. Rasband WS. ImageJ; 1997-2018. Available from: <https://imagej.nih.gov/ij/>.
28. Inc TM. MATLAB version: 23.2.0.2380103 (R2023b); 2023. Available from: <https://www.mathworks.com>.
29. Haasters F, Prall WC, Anz D, Bourquin C, Pautke C, Endres S, et al. Morphological and immunocytochemical characteristics indicate the yield of early progenitors and represent a quality control for human mesenchymal stem cell culturing. *Journal of anatomy*. 2009;214(5):759–767. doi:10.1111/j.1469-7580.2009.01065.x
30. Settleman J. Tension precedes commitment – even for a stem cell. *Mol Cell*. 2004;14(2):148–150. doi:10.1016/s1097-2765(04)00207-2.
31. Delorme B, Chateauvieux S, Charbord P. The concept of mesenchymal stem cells. *Regenerative medicine*. 2006;1(4):497–509. doi:10.2217/17460751.1.4.497.
32. Li J, Wu Z, Zhao L, Liu Y, Su Y, Gong X, et al. The heterogeneity of mesenchymal stem cells: an important issue to be addressed in cell therapy. *Stem cell research & therapy*. 2023;14:381. doi:10.1186/s13287-023-03587-y.
33. Smith JR, Pochampally R, Perry A, Hsu SC, Prockop DJ. Isolation of a highly clonogenic and multipotential subfraction of adult stem cells from bone marrow stroma. *Stem cells*. 2004;22(5):823–831. doi:10.1634/stemcells.22-5-823.
34. Frattini A, Fabbri M, Valli R, De Paoli E, Montalbano G, Gribaldo L, et al. High variability of genomic instability and gene expression profiling in different HeLa clones. *Scientific reports*. 2015;5:1–9. doi:10.1038/srep15377.
35. Liu Y, Mi Y, Mueller T, Kreibich S, Williams EG, Van Drogen A, et al. Multi-omic measurements of heterogeneity in HeLa cells across laboratories. *Nature biotechnology*. 2019;37:314–322. doi:10.1038/s41587-019-0037-y.